


First-Principles Study of the Electronic Structure and Bonding Properties of X_8C_{46} and $X_8B_6C_{40}$ (X: Li, Na, Mg, Ca) Carbon Clathrates

ANDRZEJ KOLEŻYŃSKI ^{1,2} and WOJCIECH SZCZYPKA¹

1.—Faculty of Materials Science and Ceramics, AGH University of Science and Technology, Al. Mickiewicza 30, 30-059 Kraków, Poland. 2.—e-mail: andrzej.kolezynski@agh.edu.pl

Results from theoretical analysis of the crystal structure, electronic structure, and bonding properties of C_{46} and B_6C_{40} carbon clathrates doped with selected alkali and alkaline earth metals cations (Li, Na, Mg, Ca) are presented. The *ab initio* calculations were performed by means of the WIEN2k package (full potential linearized augmented plane wave method (FP-LAPW) within density functional theory (DFT)) with PBESol and modified Becke–Johnson exchange–correlation potentials used in geometry optimization and electronic structure calculations, respectively. The bonding properties were analyzed by applying Bader’s quantum theory of atoms in molecules formalism to the topological properties of total electron density obtained from *ab initio* calculations. Analysis of the results obtained (i.e. equilibrium geometry, equation of state, cohesive energy, band structure, density of states—both total and projected on to particular atoms, and topological properties of bond critical points and net charges of topological atoms) is presented in detail.

Key words: Carbon clathrates, WIEN2k DFT calculations, electronic structure, Bader’s QTAiM analysis

INTRODUCTION

A substantial amount of research on thermoelectric materials has been devoted to silicon and germanium semiconducting clathrates, because their structure has potential from the perspective of the phonon-glass electron-crystal (PGE) concept.¹ Major developments in inorganic carbon chemistry are attracting much interest among scientists because of the possibility to synthesizing analogous carbon-based clathrates. Recently, several theoretical studies have been conducted to predict the thermodynamic,² mechanical,³ and electronic⁴ properties of carbon clathrates and the conditions used to obtain them.

Despite numerous experimental trials, carbon clathrates have not yet been synthesized, and thus theoretical predictions of their properties are wait-

ing for experimental confirmation. A wide examination and detailed analysis of how dopants located inside carbon cages affect carbon clathrate properties is a promising way of broadening current knowledge in this field. Partial substitution of carbon atoms (e.g. with silicon or boron) may also be an interesting means of determining which experimental method is potentially the most successful for obtaining stable compounds with satisfactory electronic properties.^{5–8}

Although the manner in which electronic structure affects the bulk properties of materials has been widely studied, little effort has been devoted to local interactions between atoms in the crystal lattice. Such studies may provide valuable information (complementary to electronic structure) about the correlation between the chemical bonding in a structure and properties of the bulk material, e.g. thermoelectric properties. Bader’s quantum theory of atoms in molecules (QTAiM),⁹ which is described briefly later in this paper is one of the most valuable

methods based on the topological properties of total electron density enabling such analysis of chemical bonding in a specific structure.

COMPUTATIONAL DETAILS

Ab initio calculations for a set of type I carbon clathrates were performed by use of the WIEN2k package,¹⁰ by using full potential linearized augmented plane wave (FP-LAPW) method within DFT formalism. Full optimization and electronic structure calculations were performed for the empty C_{46} clathrate and a series of X_8C_{46} and $X_8B_6C_{40}$ model structures (Fig. 1), where X = Li, Na, Mg, or Ca (space group 223, $Pm-3n$). The values chosen for the calculations were: 250 k -points ($6 \times 6 \times 6$ k -mesh within the irreducible Brillouin zone), cut-off parameter $Rk_{\max} = 7.5$, Perdew–Burke–Ernzerhof generalized gradient approximation exchange–correlation potential optimized for solids (PBESol¹¹) for optimization procedures, and modified Becke–Johnson (mBJ¹²) potential for electronic structure calculations, the values of muffin-tin radii (a.u.) (C 1.35, B 1.35, Li 1.5, Na 1.6, Mg 1.8, Ca 1.8), and the convergence criteria for SCF: $\Delta E_{\text{SCF}} \leq 10^{-5}$ (Ry) for total energy and $\Delta \rho_{\text{SCF}} \leq 10^{-5}$ (e) for electron density topology analysis. For all the optimized structures CIF files were prepared; these are included in the Electronic Supplementary Material.

Because of the inability to provide fully reliable results for single-atom energy calculations within the LAPW approach (as a result of the need to create large unit cells with single atoms to mimic isolated atoms), it is a problem to calculate reliable cohesive energies of analyzed structures by use of WIEN2k software. For this reason Crystal 14 software^{13,14} was used, and produced results comparable for zero and three-dimensional systems (in both cases orbitals were calculated as linear combinations of atom-centered Gaussian-type functions). The *ab initio* calculations of cohesive energies were conducted within DFT formalism, with GGA PBE-Sol exchange correlation potential, Fock/KS matrix mixing equal to 20%, a reciprocal lattice grid of $4 \times 4 \times 4$ (10 k points in irreducible Brillouin zone), and triple-zeta valence with polarization quality basis sets,¹⁵ optimized for specific structures. For optimization of the geometry of all the clathrates studied, the full optimization mode (optimization of cell constants and atomic positions) and the following convergence criteria: total energy difference 10^{-10} a.u., max. energy gradient and root-mean-square of the energy gradient 0.0003 a.u. and 0.00045 a.u. respectively, maximum and rms of atomic displacement 0.0018 a.u. and 0.0012 a.u. respectively, were chosen. The cohesive energies were calculated as the difference between the total energy of a given clathrate and the sum of the total atomic energies of the constituent atoms:

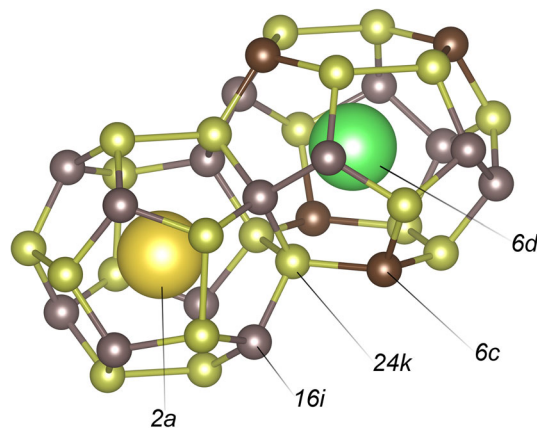
$$E_{\text{coh}} = E_{\text{bulk}} - \sum_i E_i^{\text{at}}$$


Fig. 1. Part of the X_8C_{46} clathrate structure with Wyckoff positions of atoms.

The calculated total electron density distribution in the optimized structures was used as a basis for topological analysis (within Bader’s QTAiM approach⁹) focusing on the properties of topological atoms (volume and net charge) and bond critical points (i.e. points located between two interacting atoms, characterized by a gradient of the scalar electron density field equal to zero and two negative and one positive eigenvalues of the Hessian matrix of electron density). By use of this method, information about the character of bonding interactions in a structure can be determined and physical space partitioning into adjoining atomic basins can be performed unequivocally, and thus the volume and net charge of a topological atom can be calculated. All calculations of electron density topological properties were conducted by use of Critic2 software.¹⁶

RESULTS

Density of States

Because results of calculations using the GGA potential often underestimate the band gap of semiconductors, the Tran–Blaha modified Becke–Johnson potential,¹² which is predicted to give more accurate results for such systems, was used to calculate the electronic structure of the clathrates. Calculated band gaps using both mentioned potentials are presented in Table I. For each structure, a significant increase of band gap is observed when mBJ is used; results for C_{46} were in good agreement with previously reported results of calculations performed by use of the GW approximation (5.25 eV^4).

Density of states calculated by use of the mBJ potential are presented in Fig. 2. For all doped clathrates except Mg_8C_{46} the Fermi level is located in the conduction band, which implies *n*-type conduction. For the Mg-doped C_{46} clathrate the Fermi level is located in a valence band and thus *p*-type conduction is predicted.

The vast majority of both types of charge carrier originate from carbon atoms; in the structures in which boron is present, only small number of its electrons occupy valence band states close to band gap. For all the doped structures, electrons originating from the alkali and alkaline earth atoms contribute mostly to the excited states in the conduction band. Because carbon substitution by boron leads (as expected) to lowering of the Fermi level, increasing the amount of boron will move the Fermi level even further toward the bottom of the conduction band and should, at least for alkali metal

clathrates, improve their thermoelectric properties (for which states lying within the range of a few kT from Fermi level are crucial).

Band Structure

Band structures, with band characters of specific elements in the chosen structures, are presented in Fig. 3. For C_{46} clathrates (Fig. 3f), the band gap is found to be almost exactly between Γ and X high symmetry points in the Brillouin zone, which is consistent with predictions based on calculations using the GW approximation.⁴ The Li-doped structure (Fig. 3a and b) has an indirect band gap with maximum of the valence band near the middle, between Γ and X and minimum of the conduction band (CB) at Γ .

The band structures of the Mg-doped pure carbon clathrate and of the clathrate with carbon partially substituted by boron (Fig. 3c, d, and e–g, respectively) differ substantially (and thus for these, in contrast with the others, the rigid band approximation does not hold). The former have an indirect, narrow band gap (maximum of the valence band at M, minimum of the conduction band at Γ) whereas the latter have a direct and wider band gap (at M). Moreover, the valence bands of $Mg_8B_6C_{40}$ near the Fermi level, partially filled by electrons from boron, are less dispersed than the corresponding bands for Mg_8C_{46} .

Table I. Band gaps (eV) in the electronic structures of the structures analyzed, calculated by using different DFT potentials: PBESol and mBJ

E_g	PBESol	mBJ
C_{46}	3.54	4.90
Li_8C_{46}	2.55	3.44
Na_8C_{46}	3.40	4.25
Mg_8C_{46}	0.14	0.58
Ca_8C_{46}	0.65	0.92
$Li_8B_6C_{40}$	1.87	2.82
$Na_8B_6C_{40}$	2.99	4.01
$Mg_8B_6C_{40}$	1.94	2.65
$Ca_8B_6C_{40}$	0.68	1.09

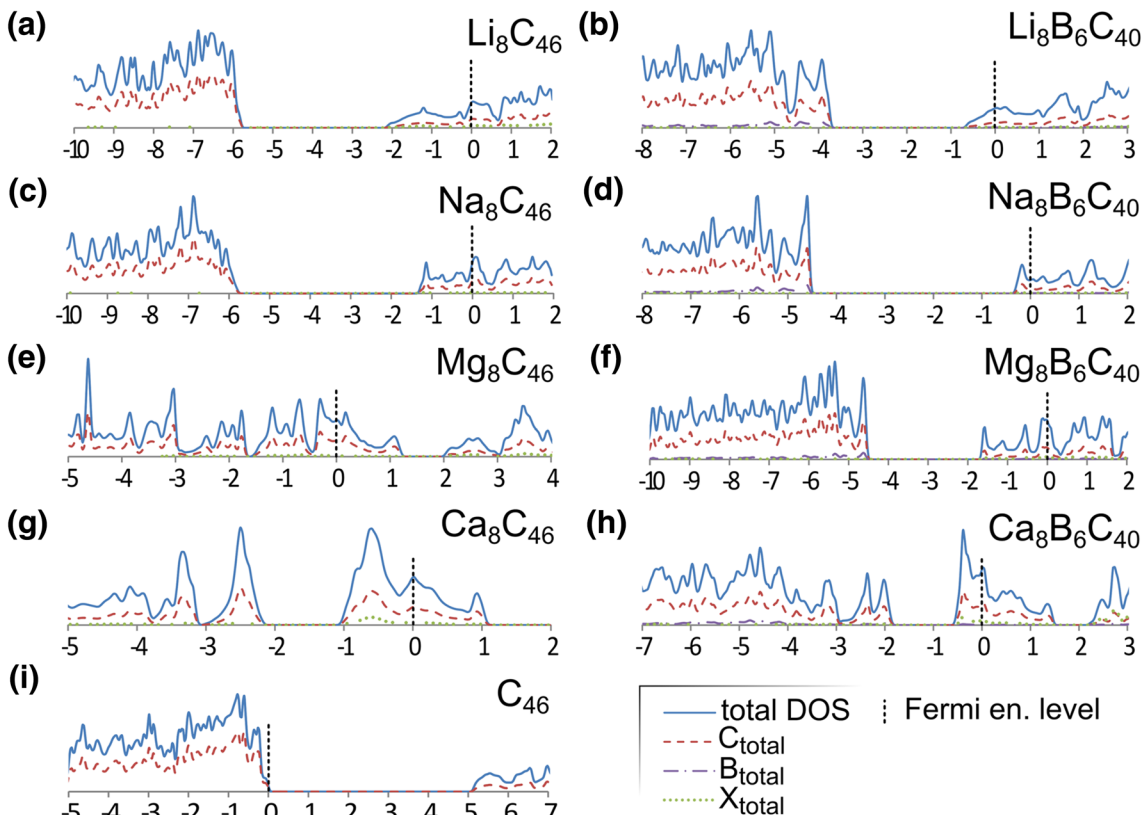


Fig. 2. Total and projected density of states near the Fermi level for all the structures analyzed (energy, on the x-axes, is in eV).

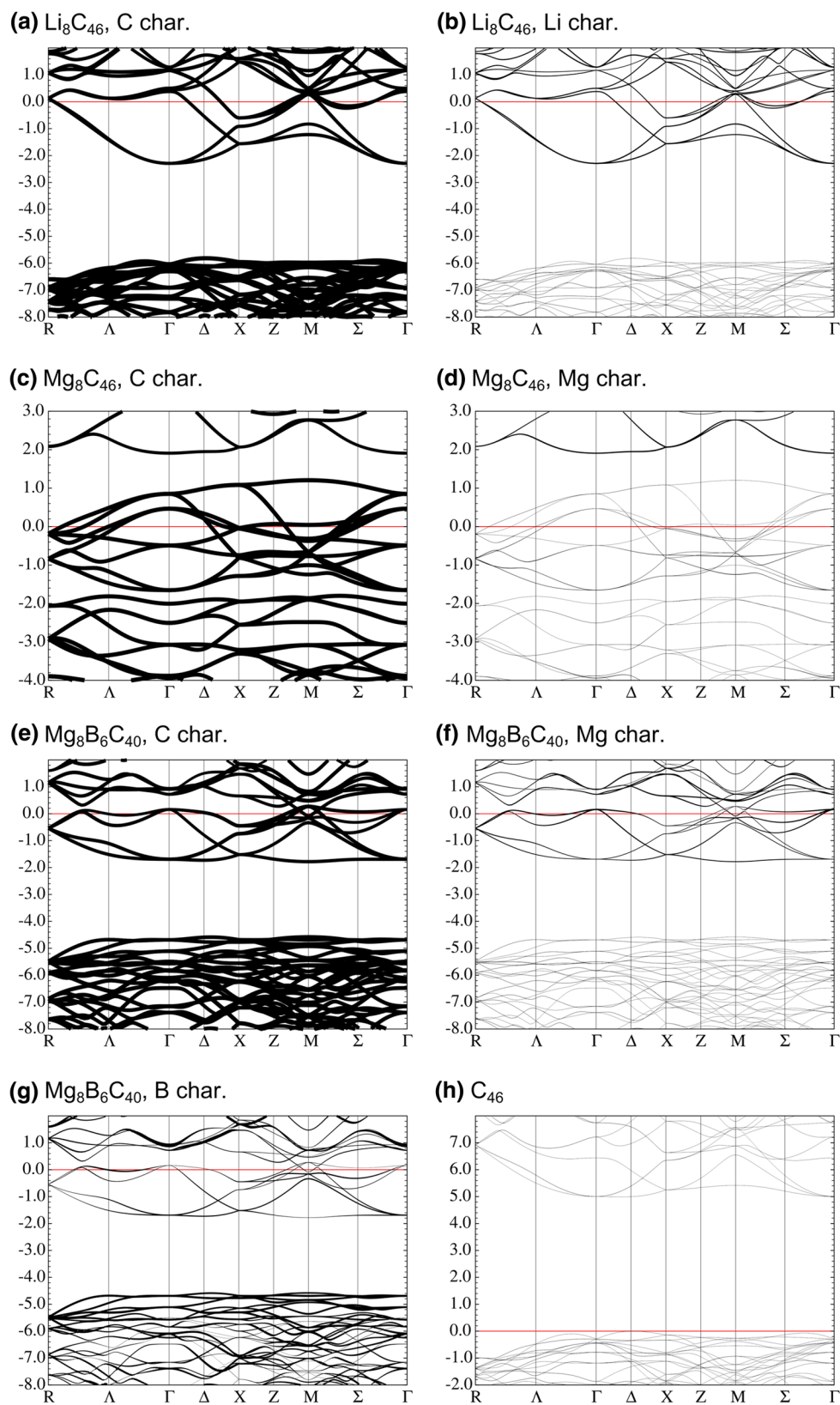


Fig. 3. Band structure, with band characters emphasized, calculated for (a, b) Li_8C_{46} , (c, d) Mg_8C_{46} , (e–g) $Mg_8B_6C_{40}$ and (h) C_{46} clathrates. (In (g) the widths of bands corresponding to boron were tripled for easier recognition). Energies on the x-axes (eV) are set to zero for the Fermi level.

The electronic structure of the Mg-doped pure clathrate is markedly different from that of the other systems because of severe distortion of its crystal structure in comparison with C_{46} . This structure modification (described more extensively below, in the section “[Electron Density Topology](#)”) resulted in significant changes of C–C bonds lengths. Because the energy states of carbon atoms, the majority of the atoms present, determine the properties of valence bands located close to the top of the valence band (VB), strong modification of their surroundings caused substantial changes in the dispersion of the respective bands. As a result, the Fermi level was found to be inside the VB. By analogy, doping the carbon clathrate with calcium also results in substantial modification of the electronic structure, but the resulting compound does not change its conductivity type (in our opinion this difference in comparison with magnesium clathrate is mainly because of the much larger ionic radius and the smaller amount of charge transferred to the carbon atoms).

Effective Masses

Additional calculations were performed to estimate the effective masses of carriers near the band

gap (a parabolic dispersion relationship was assumed). To obtain reliable estimates of effective masses, a new set of k -points located in the proximity of the extremes of the VB and CB were prepared in such a way that for every extreme point two or three paths toward high-symmetry points in the Brillouin zone were probed by 50 k -points up to $1/10$ the length of $2\pi/a_0$ (multiplied by $\sqrt{2}$ or $\sqrt{3}$ for diagonal paths) from the respective extreme. These sets were used for LAPW calculations, and appropriate fragments of the respective bands from the resulting band structures were extracted to fit the analytical parabolic function from which the effective masses were calculated.

The results of this approximation are presented in Table II.

For the structures containing boron atoms, a slight increase of holes masses is observed in comparison with X_8C_{46} systems (except for $Mg_8B_6C_{40}$). Compared with the pure carbon clathrate heavier holes appear for Mg_8C_{46} and all $X_8B_6C_{40}$ structures whereas for the effective masses of electrons no such clear tendencies can be observed. Moreover, for Na-doped clathrates very “flat” bands were observed which made calculation of effective masses problematic, because of numerical noise (marked “a” in Table II).

Table II. Effective masses of electrons and holes calculated as described in text (scaled by m_0)

	<i>h</i>			<i>e</i>		
C_{46}	$\Delta_e \rightarrow \Gamma$ (0.14) -0.84		$\Delta_e \rightarrow X$ (0.12) -1.21	$\Delta_e \rightarrow \Gamma$ (0.10) 3.74		$\Delta_e \rightarrow X$ (0.16) 1.52
Li_8C_{46}	$\Delta_e \rightarrow \Gamma$ (0.13) -0.83		$\Delta_e \rightarrow X$ (0.12) -1.05	$\Gamma \rightarrow \Lambda$ 0.65 0.65 0.65	$\Gamma \rightarrow \Delta_e$ 1.53 0.5 0.5	$\Gamma \rightarrow \Sigma$ 0.77 0.76 0.5
Na_8C_{46}	$M \rightarrow Z$ -1.24	$M \rightarrow \Sigma$ -1.23	$M \rightarrow T$ -0.91	$\Delta_e \rightarrow \Gamma$ (0.05) 20 ^a		$\Delta_e \rightarrow X$ (0.19) 3.3
Mg_8C_{46}	$M \rightarrow Z$ -3.05	$M \rightarrow \Sigma$ -2.91	$M \rightarrow T$ -0.24	$\Gamma \rightarrow \Lambda$ 1.77	$\Gamma \rightarrow \Delta_e$ 2.46	$\Gamma \rightarrow \Sigma$ 2.05
Ca_8C_{46}	$M \rightarrow Z$ -1.15	$M \rightarrow \Sigma$ -1.2	$M \rightarrow T$ -1.06	$M \rightarrow Z$ 0.93	$M \rightarrow \Sigma$ 0.73	$M \rightarrow R$ 1.96
$Li_8B_6C_{40}$	$\Delta_e \rightarrow \Gamma$ (0.13) -1.84		$\Delta_e \rightarrow X$ (0.11) -1.3	$\Gamma \rightarrow \Lambda$ 0.83 0.68 0.68	$\Gamma \rightarrow \Delta_e$ 1.49 0.58 0.58	$\Gamma \rightarrow \Sigma$ 0.93 0.75 0.57
$Na_8B_6C_{40}$	$\Delta_e \rightarrow \Gamma$ (0.13) -1.94		$\Delta_e \rightarrow X$ (0.10) -1.43	$\Gamma \rightarrow \Lambda$ 2.9 0.85 0.85	$\Gamma \rightarrow \Delta_e$ 17.15 ^a 0.76 0.76	$\Gamma \rightarrow \Sigma$ 4.29 0.9 0.75
$Mg_8B_6C_{40}$	$M \rightarrow Z$ -2.26	$M \rightarrow \Sigma$ -2.19	$M \rightarrow T$ -0.87	$M \rightarrow Z$ 1.9	$M \rightarrow \Sigma$ 2.32	$M \rightarrow T$ 0.58
$Ca_8B_6C_{40}$	$M \rightarrow Z$ -3.27 -1.52	$M \rightarrow \Sigma$ -3.44 -1.4	$M \rightarrow T$ -0.56 -0.81	$M \rightarrow Z$ 1.15	$M \rightarrow \Sigma$ 1.36	$M \rightarrow R$ 1.39

Values in parentheses indicate distances between Δ_e and Γ/X k points (in Bohr⁻¹).^aValues calculated with high uncertainty (see text for details).

Cohesive Energies

To check whether introduction of boron into the clathrate structure is favorable thermodynamically, the cohesive energies of structures with and without boron were calculated and compared. The results of such calculations are presented in Table III. Because ΔE_{coh} (see the footnote of Table III for details) is negative for all pairs of structures with the same guest atom, it can be concluded that the presence of boron in the clathrate is stabilizing this system as a whole.

It is also worth noticing that the calculated cohesive energies of structures with magnesium as guest atom are substantially greater than those obtained for other structures, reaching approximately 50% more in comparison with the empty carbon clathrate C_{46} . This might be a result of the specific properties of magnesium cations—the quite large effective charge and small ionic radius leading

to stronger electromagnetic interactions with the surrounding atoms, followed by a bigger charge flow and total energy decrease, resulting in increased structure stabilization.

Electron Density Topology

The total electron density distribution results obtained from FP-LAPW SCF calculations were analyzed within Bader's QTAIM model. The calculated net charges and the volumes of specific topological atoms for all the structures are presented in Table IV. It follows from these results that introduction of boron into the carbon clathrate (substitution of C_{6c} atoms) strongly increases the negative charges on carbon (especially for C_{24k} bonded directly to B_{6c}), as a result of boron's lower electronegativity. Also, the changes of guest atom net charges are negligibly small, which suggests that the presence of boron in a clathrate structure (at

Table III. Cohesive energies calculated for the structures analyzed

	E_{tot}	ΣE_{at}	E_{coh}	ΔE_{coh}
C_{46}	-1744.083	-1724.361	-19.722	-
Li_8C_{46}	-1803.137	-1781.075	-22.063	-
Na_8C_{46}	-3037.042	-3016.168	-20.874	-
Mg_8C_{46}	-3332.415	-3303.054	-29.360	-
Ca_8C_{46}	-7153.926	-7132.473	-21.453	-
$Li_8B_6C_{46}$	-1724.420	-1702.152	-22.269	-0.206
$Na_8B_6C_{46}$	-2958.550	-2937.245	-21.305	-0.430
$Mg_8B_6C_{46}$	-3253.717	-3224.131	-29.586	-0.225
$Ca_8B_6C_{46}$	-7075.497	-7053.550	-21.946	-0.493

Cohesive energy was calculated as the difference between the total energy of a given structure and the sum of the energies of the isolated atoms $E_{\text{coh}} = E_{\text{tot}} - \Sigma E_{\text{at}}$. ΔE_{coh} is the difference between the cohesive energies of structures with and without boron but with the same metallic dopant: $\Delta E_{\text{coh}} = E_{\text{coh}}(X_8B_6C_{40}) - E_{\text{coh}}(X_8C_{46})$ (all values are in a.u.).

Table IV. Net charges and volumes of topological atoms in the structures analyzed (in e and Bohr³, respectively) calculated at bond critical points (BCP)

Atom _{Wyck.}	C_{46}	Li_8C_{46}	Na_8C_{46}	Mg_8C_{46}	Ca_8C_{46}	$Li_8B_6C_{40}$	$Na_8B_6C_{40}$	$Mg_8B_6C_{40}$	$Ca_8B_6C_{40}$
C_{6c}/B_{6c}									
q	-0.008 ^a	-0.161	-0.076	-0.090	-0.195	1.642	1.609	1.530	1.609
Ω	45.02	43.84	43.20	44.59	45.91	20.44	20.35	21.53	20.03
C_{16i}									
q	0.020	-0.142	-0.078	-0.107	-0.157	-0.094	-0.104	-0.188	-0.112
Ω	40.70	40.42	40.28	39.81	42.19	41.87	41.93	42.51	40.96
C_{24k}									
q	-0.015	-0.239	-0.193	-0.463	-0.237	-0.642	-0.612	-0.800	-0.769
Ω	45.15	44.42	45.00	53.05	43.17	53.13	52.11	54.72	56.79
A_{2a}									
q	-	0.850	0.816	1.696	1.165	0.875	0.825	1.704	1.274
Ω	-	15.92	32.45	28.67	52.68	15.71	31.89	26.17	54.97
A_{6d}									
q	-	0.867	0.819	1.656	1.202	0.889	0.845	1.630	1.351
Ω	-	19.08	39.12	34.02	61.77	20.14	40.25	33.59	66.87

^aCarbon atom at Wyckoff position 6d.

Table V. BCP properties in the structures analyzed, calculated from the total electron density topology: multiplicity M , bond length R (in Å), electron density $\rho(r_{\text{BCP}})$ and Laplacian $\nabla^2\rho(r_{\text{BCP}})$ at BCP (in a.u.)

	Bond	M	R	$\rho_{\text{BCP}}(r)$	$\nabla^2\rho(r)$
C_{46}					
1	$\text{C}_{24\text{k}}-\text{C}_{24\text{k}}$	12	1.562	0.229	-0.563
2	$\text{C}_{16\text{i}}-\text{C}_{24\text{k}}$	48	1.518	0.252	-0.713
3	$\text{C}_{16\text{i}}-\text{C}_{16\text{i}}$	8	1.495	0.264	-0.799
4	$\text{C}_{6\text{d}}-\text{C}_{24\text{k}}$	24	1.544	0.239	-0.625
Na_8C_{46}					
1	$\text{C}_{24\text{k}}-\text{C}_{24\text{k}}$	12	1.793	0.145	-0.111
2	$\text{C}_{16\text{i}}-\text{C}_{24\text{k}}$	48	1.582	0.218	-0.470
3	$\text{C}_{16\text{i}}-\text{C}_{16\text{i}}$	8	1.543	0.235	-0.598
4	$\text{C}_{6\text{c}}-\text{C}_{24\text{k}}$	24	1.613	0.205	-0.404
5	$\text{Na}_{6\text{d}}-\text{C}_{24\text{k}}$	48	2.393	0.023	0.118
6	$\text{Na}_{2\text{a}}-\text{C}_{24\text{k}}$	24	2.293	0.029	0.169
7	$\text{Na}_{2\text{a}}-\text{C}_{16\text{i}}$	16	2.246	0.031	0.180
Mg_8C_{46}					
1	$\text{C}_{24\text{k}}-\text{C}_{24\text{k}}$	12	2.391	0.047	0.056
2	$\text{C}_{16\text{i}}-\text{C}_{24\text{k}}$	48	1.533	0.236	-0.587
3	$\text{C}_{16\text{i}}-\text{C}_{16\text{i}}$	8	1.605	0.204	-0.407
4	$\text{C}_{6\text{c}}-\text{C}_{24\text{k}}$	24	1.582	0.211	-0.422
5	$\text{Mg}_{6\text{d}}-\text{C}_{24\text{k}}$	24	2.386	0.030	0.096
6	$\text{Mg}_{2\text{a}}-\text{C}_{16\text{i}}$	16	2.282	0.030	0.130
Li_8C_{46}					
1	$\text{C}_{24\text{k}}-\text{C}_{24\text{k}}$	12	1.644	0.195	-0.315
2	$\text{C}_{16\text{i}}-\text{C}_{24\text{k}}$	48	1.563	0.231	-0.512
3	$\text{C}_{16\text{i}}-\text{C}_{16\text{i}}$	8	1.520	0.252	-0.656
4	$\text{C}_{6\text{c}}-\text{C}_{24\text{k}}$	24	1.592	0.218	-0.445
5	$\text{Li}_{2\text{a}}-\text{C}_{24\text{k}}$	24	2.230	0.022	0.118
6	$\text{Li}_{2\text{a}}-\text{C}_{16\text{i}}$	16	2.185	0.023	0.123
7	$\text{Li}_{6\text{d}}-\text{bcpl}^{\text{a}}$	24	2.144	0.018	0.086
Ca_8C_{46}					
1	$\text{C}_{24\text{k}}-\text{C}_{24\text{k}}$	12	2.336	0.054	0.058
2	$\text{C}_{16\text{i}}-\text{C}_{24\text{k}}$	48	1.553	0.227	-0.472
3	$\text{C}_{16\text{i}}-\text{C}_{16\text{i}}$	8	1.573	0.219	-0.450
4	$\text{C}_{6\text{c}}-\text{C}_{24\text{k}}$	24	1.573	0.216	-0.398
5	$\text{Ca}_{6\text{d}}-\text{C}_{24\text{k}}$	24	2.420	0.046	0.131
6	$\text{Ca}_{2\text{a}}-\text{C}_{16\text{i}}$	16	2.301	0.048	0.190
$\text{Na}_8\text{B}_6\text{C}_{40}$					
1	$\text{C}_{24\text{k}}-\text{C}_{24\text{k}}$	12	1.682	0.178	-0.271
2	$\text{C}_{16\text{i}}-\text{C}_{24\text{k}}$	48	1.597	0.212	-0.449
3	$\text{C}_{16\text{i}}-\text{C}_{16\text{i}}$	8	1.587	0.221	-0.517
4	$\text{B}_{6\text{c}}-\text{C}_{24\text{k}}$	24	1.685	0.145	-0.196
5	$\text{Na}_{6\text{d}}-\text{C}_{24\text{k}}$	48	2.407	0.022	0.118
6	$\text{Na}_{2\text{a}}-\text{C}_{24\text{k}}$	24	2.266	0.031	0.182
7	$\text{Na}_{2\text{a}}-\text{C}_{16\text{i}}$	16	2.253	0.030	0.186
$\text{Mg}_8\text{B}_6\text{C}_{40}$					
1	$\text{C}_{24\text{k}}-\text{C}_{24\text{k}}$	12	1.741	0.156	-0.154
2	$\text{C}_{16\text{i}}-\text{C}_{24\text{k}}$	48	1.597	0.208	-0.411
3	$\text{C}_{16\text{i}}-\text{C}_{16\text{i}}$	8	1.583	0.219	-0.496
4	$\text{B}_{6\text{c}}-\text{C}_{24\text{k}}$	24	1.678	0.143	-0.175
5	$\text{Mg}_{6\text{d}}-\text{C}_{24\text{k}}$	48	2.427	0.026	0.090
6	$\text{Mg}_{2\text{a}}-\text{C}_{24\text{k}}$	24	2.284	0.032	0.162
$\text{Li}_8\text{B}_6\text{C}_{40}$					
1	$\text{C}_{24\text{k}}-\text{C}_{24\text{k}}$	12	1.611	0.203	-0.385
2	$\text{C}_{16\text{i}}-\text{C}_{24\text{k}}$	48	1.572	0.221	-0.489
3	$\text{C}_{16\text{i}}-\text{C}_{16\text{i}}$	8	1.569	0.230	-0.547
4	$\text{B}_{6\text{c}}-\text{C}_{24\text{k}}$	24	1.661	0.149	-0.182
5	$\text{Li}_{6\text{d}}-\text{C}_{24\text{k}}$	48	2.354	0.015	0.078
6	$\text{Li}_{2\text{a}}-\text{C}_{24\text{k}}$	24	2.220	0.021	0.113
7	$\text{Li}_{2\text{a}}-\text{C}_{16\text{i}}$	16	2.205	0.021	0.114
$\text{Ca}_8\text{B}_6\text{C}_{40}$					
1	$\text{C}_{24\text{k}}-\text{C}_{24\text{k}}$	12	2.277	0.059	0.044

Table V. continued

	Bond	M	R	$\rho_{\text{BCP}}(r)$	$\nabla^2\rho(r)$
2	$C_{16i}-C_{24k}$	48	1.577	0.215	-0.462
3	$C_{16i}-C_{16i}$	8	1.670	0.184	-0.303
4	$B_{6c}-C_{24k}$	24	1.673	0.142	-0.154
5	$Ca_{6d}-C_{24k}$	24	2.541	0.035	0.104
6	$Ca_{2a}-C_{24k}$	24	2.422	0.042	0.163
7	$Ca_{2a}-C_{16i}$	16	2.336	0.045	0.186

^aBCP between Li nuclear critical point and BCP of $C_{24k}-C_{24k}$ bond.

least in the configuration analyzed) does not substantially affect charge transfer between guest and host atoms, and charge flow is confined mostly to the host sublattice.

Valuable information about the interactions between guest atoms and the clathrate network can be obtained by analyzing of electron density properties at bond critical points (Table V). All of these points related to X-C bonds are characterized by small values of electron density and relatively high and positive Laplacian, which is characteristic for weak closed-shell interactions, with the highest electron density at BCP in Ca-doped structures (electron density approximately one and a half times greater than for the other guest atoms). The lengths of these bonds differ only slightly from each other, however. All these features suggest that guest atoms are loosely bonded to clathrate networks in accordance with one of the requirements of the PGEC concept mentioned by Cahill et al.¹⁷

Most of the C-C bonds and all C-B bonds have evident covalent character (very high electron density and strongly negative Laplacian at their critical points). However, for Mg_8C_{46} , Ca_8C_{46} , and $Ca_8B_6C_{40}$ the respective values of the Laplacians for $C_{24k}-C_{24k}$ BCP shift from negative (but less negative than for other C-C bonds) to positive, whereas electron density decreases (these C-C bonds are much longer than the others and their lengths exceed 2 Å). This indicates that these particular bonds are relatively weak with notable ionic character.

The C_{20} cages of Li_8C_{46} (a), Mg_8C_{46} (b), and $Mg_8B_6C_{40}$ (c) are depicted in Fig. 4. In the first of these all the C-C bonds are of similar length and the lithium atom is surrounded nearly equally by all the carbon atoms, so that free motion of the guest atom is strictly limited to the interior space of the cage. The situation is different for (b): the $C_{24k}-C_{24k}$ bond (with closed-shell interactions in this case) is much longer than other C-C bonds and the whole cage becomes less rigid. This is an important property of these structures, for they can easier accommodate guest cations rattling in a direction perpendicular to the bond (because of a momentary bond elongation accompanied by structure deformation) which can result in stronger scattering of respective phonons. Introduction of boron to the

clathrate network doped with magnesium (c) results in partial stabilization of this network and, again, the whole cage is closed by covalent bonds. Similar changes are observed in structures with calcium atoms, but the stabilization effect of boron is not so distinct here ($Ca_8B_6C_{40}$ $C_{24k}-C_{24k}$ bonds are still substantially weaker). Moreover, no direct correlation between the net charge of the C_{24k} topological atom and the $C_{24k}-C_{24k}$ bond length indicates that the main reason for cage-structure changes in these carbon clathrates must be the different properties of each guest atom.

Because in the pure C_{46} carbon clathrate the $C_{24k}-C_{24k}$ bond is the weakest (it is the longest and has the lowest electron density at the BCP) it can be stretched more easily when the cages are filled. This is observed for all the systems analyzed; for three, however (Mg_8C_{46} , Ca_8C_{46} , and $Ca_8B_6C_{40}$), elongation of this particular bond is so high that it changes its character from strong covalent to ionic. From a chemical perspective, two important effects may be involved: charge transfer between the doped metal and the host structure and the size of the ionic radii of the guest cations. Alkaline earth metals donate more electrons than alkali metals to neighboring carbon atoms, mostly to C_{24k} . This is particularly evident for magnesium (over 1.6 of positive net charge of Mg and also the highest negative charge of C_{24k} ; Table IV). Accumulation of electrons at carbon atoms might be the reason for slackening of the $C_{24k}-C_{24k}$ bond—more negatively charged atoms are pushed away from each other and simultaneously “pulled” toward less charged neighbors. Introduction of less electronegative boron into the 6c site results in polarized covalent $B_{6c}-C_{24k}$ bonds, longer than the corresponding $C_{6c}-C_{24k}$ bonds in pure and doped carbon clathrates. The negative charge of C_{24k} strongly increases, but further elongation of $C_{24k}-C_{24k}$ does not occur. On the contrary, it shrinks and becomes covalent and strong again, possibly because of weaker “pulling” of C_{24k} by boron and greater peer attraction of C_{24k} . Because the magnesium cation is very small (ionic radius similar to that of lithium) it does not prevent this “cage closing” process. The situation is different for calcium-doped clathrates: the calcium cation is much larger than that of magnesium (it is, in fact,

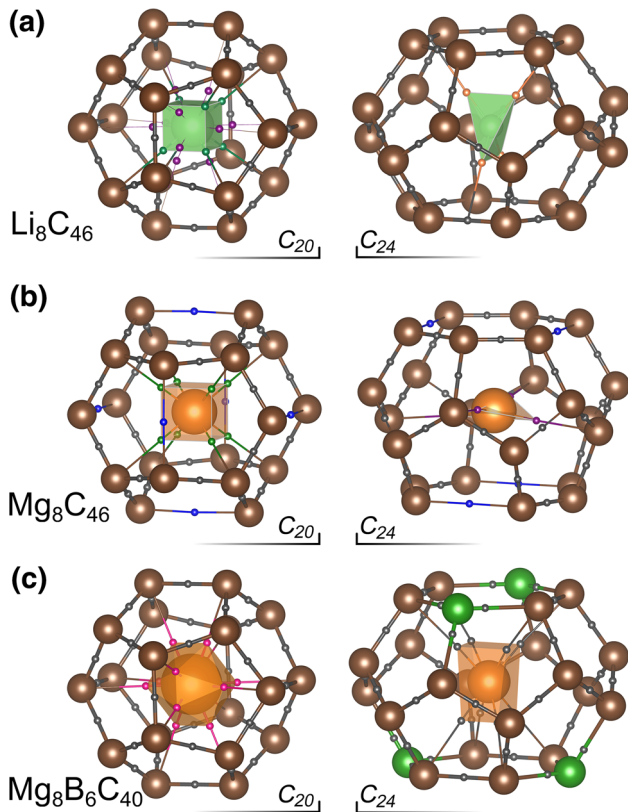


Fig. 4. C_{20} and C_{24} cages of chosen structures (as written on the left) with guest atoms inside and BCP marked as small spheres on bonds. One can observe elongation of $C_{24k}-C_{24k}$ bonds in (b). This effect is not observed for the Mg-doped structure with boron atoms (c).

the largest cation of those studied here). Ca donates many fewer electrons than Mg (1.2 positive net charge), so in the Ca-doped clathrate the charge of C_{24k} is comparable with the respective ones in the Li and Na-doped clathrates. The calcium cation, significantly larger than the other cations analyzed, stretches the carbon cage from inside, resulting in an increase of C–C bond lengths (and, because in the original empty carbon clathrate the weakest bond is the $C_{24k}-C_{24k}$ bond, it is the most elongated). Because of the size of the calcium cation, exchanging C_{6c} carbon atoms with boron results in very slight shrinkage of the $C_{24k}-C_{24k}$ bond only.

Because of these effects one can expect similar crystal structure modification (cage opening) for carbon clathrates containing other elements, for example Zn, Al, and Ga. Because the Pauling radius for zinc is 74 pm (for Zn^{2+}) the resulting Zn-guested clathrate should have properties intermediate between those of magnesium (65 pm) and calcium (99 pm). For Al (50 pm for Al^{3+}) and Ga (62 pm for Ga^{3+}) the ionic radii are even smaller than that of magnesium and the formal charge is higher (+3), so even larger structure modification can be expected,

although further studies are necessary to confirm this inference.

CONCLUSIONS

Results of *ab initio* calculations for the pure type I carbon clathrate C_{46} , for model structures containing different guest atoms (X_8C_{46}), and for analogous structures with carbon partially substituted by boron ($X_8B_6C_{40}$) were analyzed from the perspective of the electronic properties (density of states, total and projected on to constituent atoms, band structure, and effective masses of carriers) and the topology of the total electron density (properties of bond critical points, net charges, and volumes of topological atoms). Calculated electronic structures showed that all the doped clathrates studied here should have *n*-type conducting character (except Mg_8C_{46} , for which *p*-type conduction should be observed). Apart from shifting the Fermi level to lower energies, introduction of boron does not substantially change the band structures of systems analyzed (except for the Mg-doped clathrate), in agreement with the rigid band approximation. When constructing thermoelectric modules it is preferable to use *n*-type and *p*-type materials with properties as similar as possible; from this perspective the possibility of changing the conducting character of the Mg-doped clathrate, merely by partial substitution of carbon with boron, suggests this system could be promising candidate for further investigation focusing on the effect of the type, amount, and location of the dopant within the carbon sublattice on the electronic structures of such clathrates.

Carbon clathrates with calcium and magnesium as guest atoms have a tendency toward substantial modification of their structure (with lengthening of some of C–C bonds accompanied by weakening and character change to ionic); as a result they should accommodate guest atom rattling much more easily. This may lead to increased phonon scattering and, therefore, reduced lattice thermal conductivity. Modification of a clathrate structure can be suppressed by introduction of boron into the host sublattice, as was observed for the Mg-doped system.

These results show that type I carbon clathrates doped with alkali or alkaline earth metals (especially the latter), if successfully synthesized, could be considered as potential thermoelectric materials; however, additional investigation of structures with other guest cations (and with other host lattice dopants) is necessary to confirm this.

ACKNOWLEDGEMENTS

This research was supported by Polish National Science Center, Grant No. UMO-2013-09/B/ST8/02043 and in part by PL-Grid Infrastructure.

OPEN ACCESS

This article is distributed under the terms of the Creative Commons Attribution 4.0 International License (<http://creativecommons.org/licenses/by/4.0/>), which permits unrestricted use, distribution, and reproduction in any medium, provided you give appropriate credit to the original author(s) and the source, provide a link to the Creative Commons license, and indicate if changes were made.

ELECTRONIC SUPPLEMENTARY MATERIAL

The online version of this article (doi: [10.1007/s11664-015-4028-6](https://doi.org/10.1007/s11664-015-4028-6)) contains supplementary material, which is available to authorized users.

REFERENCES

1. G.S. Nolas, J.L. Cohn, G.A. Slack, and S.B. Schujman, *Appl. Phys. Lett.* 73, 178 (1998).
2. J.-T. Wang, C. Chen, D.-S. Wang, H. Mizuseki, and Y. Kawazoe, *J. Appl. Phys.* 107, 063507 (2010).
3. X. Blase, P. Gillet, A. San Miguel, and P. Mélinon, *Phys. Rev. Lett.* 92(21), 215505 (2004).
4. X. Blasé, *Phys. Rev. B* 67, 035211 (2003).
5. M. Bernasconi, S. Gaito, and G. Benedek, *Phys. Rev. B* 61, 12689 (2000).
6. F. Zipoli, M. Bernasconi, and G. Benedek, *Phys. Rev. B* 74, 205408 (2006).
7. N. Rey, A. Muñoz, P. Rodríguez-Hernández, and A. San Miguel *J. Phys. Condens. Matter.* 20, 215218 (2008) <http://iopscience.iop.org/article/10.1088/0953-8984/20/21/215218/meta>.
8. D. Connétable, *Phys. Rev. B* 82, 075209 (2010).
9. R.F.W. Bader, *Atoms in Molecules: A Quantum Theory* (Clarendon Press, Oxford, 1990).
10. P. Blaha, K. Schwarz, G.K.H. Madsen, D. Kvasnicka, and J. Luitz, *WIEN2K: An Augmented Plane Wave Plus Local Orbitals Program for Calculating Crystal Properties* (Vienna Technological University, Vienna, 2001).
11. J.P. Perdew, A. Ruzsinszky, G.I. Csonka, O.A. Vydrov, G.E. Scuseria, L.A. Constantin, X. Zhou, and K. Burke, *Phys. Rev. Lett.* 100, 136406 (2008).
12. F. Tran and P. Blaha, *Phys. Rev. Lett.* 102, 226401 (2009).
13. R. Dovesi, R. Orlando, A. Erba, C.M. Zicovich-Wilson, B. Civalleri, S. Casassa, L. Maschio, M. Ferrabone, M.D.L. Pierre, P. D'Arco, Y. Noël, M. Causà, M. Rérat, and B. Kirtman, *Int. J. Quantum Chem.* 114, 1287 (2014).
14. R. Dovesi, V.R. Saunders, C. Roetti, R. Orlando, C.M. Zicovich-Wilson, F. Pascale, B. Civalleri, K. Doll, N.M. Harrison, I.J. Bush, P. D'Arco, M. Llunell, M. Causà, and Y. Noël, *CRYSTAL14 User's Manual* (University of Torino, Torino, 2014).
15. M.F. Peintinger, D. Vilela, Oliveira, and T. Bredow, *J. Comput. Chem.* 34(6), 451 (2013).
16. A. Otero-de-la-Roza, M. Blanco, A.M. Pendás, and V. Luaña, *Comput. Phys. Commun.* 160(1), 157 (2009).
17. D.G. Cahill, S.K. Watson, and R.O. Pohl, *Phys. Rev. B* 46, 6131 (1992).